



## Magnetic properties and catalytic performance of iron-containing mesoporous molecular sieves

Verónica R. Elías<sup>a,e</sup>, Marcos I. Oliva<sup>b,e</sup>, Silvia E. Urreta<sup>b</sup>, Silvia P. Silveti<sup>b</sup>, Karim Sapag<sup>c,e</sup>, Azucena M. Mudarra Navarro<sup>d,e</sup>, Sandra G. Casuscelli<sup>a,e</sup>, Griselda A. Eimer<sup>a,e,\*</sup>

<sup>a</sup> Centro de Investigación y Tecnología Química (CITEQ), Universidad Tecnológica Nacional, Facultad Regional Córdoba, Maestro López esq. Cruz Roja Argentina 5016, Córdoba, Argentina

<sup>b</sup> Facultad de Matemática, Astronomía y Física (FAMAF), Universidad Nacional de Córdoba, Ciudad Universitaria, 5000 Córdoba, Argentina

<sup>c</sup> Instituto de Física Aplicada – CONICET, Universidad Nacional de San Luis, Chacabuco 917, 5700 San Luis, Argentina

<sup>d</sup> Dpto. de Física-IFLP, Facultad de Ciencias Exactas, Universidad Nacional de La Plata. C.C. 67, 1900 La Plata, Argentina

<sup>e</sup> CONICET, Argentina

### ARTICLE INFO

#### Article history:

Received 3 November 2009

Received in revised form 23 March 2010

Accepted 24 March 2010

Available online 31 March 2010

#### Keywords:

Iron

Mesoporous molecular sieves

Magnetic properties

Cyclohexene oxidation

Reduction

Allylic oxidation products

### ABSTRACT

Fe-containing mesoporous molecular sieves were synthesized by the wet impregnation method with two different metallic loadings. The resulting iron oxide/silica composites were then submitted to a reduction treatment for 6 h at 873 K, under H<sub>2</sub> flow. The microstructure of both, the Si-MCM-41 host and the impregnated composites were characterized by XRD, N<sub>2</sub> adsorption, DRUV-vis and Mössbauer spectroscopy. The magnetic behavior of each microstructure was characterized by the magnetization dependence on the magnetic field (up to 1.5 T) and temperature (between 5 and 300 K). The catalytic performance was tested for cyclohexene oxidation by hydrogen peroxide and further correlated with the observed magnetic properties. It was found that the reduction treatment largely affects the selectivity to reaction products, leading to catalysts exhibiting a selectivity of 80% towards the allylic oxidation products. This is attributed to a large free radical generation arising from the interaction between the hydrogen peroxide and the partially reduced iron species (mainly Fe<sup>0</sup> and Fe<sub>3</sub>O<sub>4</sub>), exhibiting superparamagnetic and/or ferromagnetic character.

© 2010 Elsevier B.V. All rights reserved.

### 1. Introduction

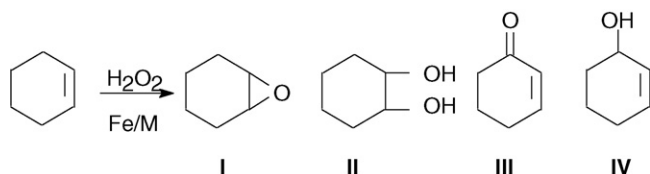
Since their discovery, the MCM-41 molecular sieves have been the basis of different catalysts of spread use in industrial processes. Their special features of high surface areas (>1000 m<sup>2</sup>/g) and highly ordered porous structure (with pore diameter between 2 and 10 nm) confer these materials a high adsorption capacity even for large molecules. The surface of the MCM-41 materials may be modified by inserting different transition metals, and the resulting catalysts are applied to numerous chemical reactions, among which special attention has been paid to the oxidation of organic substrates [1–4]. In the fine chemical industry, the selective oxidation reactions are carried out with significant amounts of transition metals and organic peroxyacids as reactive; the use of modified MCM-41 type molecular sieves emerged as an interesting option for the development of environ compatible processes. In addition, the diluted hydrogen peroxide (H<sub>2</sub>O<sub>2</sub>) is one of the most conve-

nient oxidants in use due to its easy manipulation, high active oxygen content and the absence of by-products [5]. In this context, the oxidation reactions of organic compounds, mainly bulky olefins, have gained interest [1]. Among the studied olefins, the cyclohexene is frequently used to evaluate the redox ability of modified MCM-41 using H<sub>2</sub>O<sub>2</sub> as oxidant [6]. Scheme 1 shows the typical products of this reaction. The cyclohexene oxide (**I**), generated by the heterolitic epoxidation of the cyclohexene double bond and the 1,2-cyclohexanediol (**II**) side product formed by hydrolysis of the epoxide ring, generally reflect a concerted process. The allylic oxidation products, 2-cyclohexen-1-one (**III**) and 2-cyclohexen-1-ol (**IV**), are often ascribed to a homolytic radical path [7,8].

The introduction of Fe into the molecular sieves has received much attention because of its activity in alkylation and oxidation reactions [1,2,9]. The mesoporous molecular sieves are generally constituted by diamagnetic units as carbon or silica [2] and the incorporation of magnetic ions/species in different oxidation states may lead to special catalytic behavior. In this sense, the development of molecular sieves with magnetic properties found wide application in processes of magnetic separation, transport of adsorbed compounds in a magnetic field [3,4], in the development

\* Corresponding author at: CITEQ, FRC, Maestro López esq. Cruz Roja Argentina 5016, Córdoba, Argentina. Tel.: +54 351 4690585.

E-mail address: [geimer@scdt.frc.utn.edu.ar](mailto:geimer@scdt.frc.utn.edu.ar) (G.A. Eimer).



**Scheme 1.** Products of cyclohexene oxidation by hydrogen peroxide. Cyclohexene oxide (I), 1,2-cyclohexanediol (II), 2-cyclohexen-1-one (III) and 2-cyclohexen-1-ol (IV).

of magneto-chemical sensors [10–12], as high density magnetic recording supports and other nano-devices [13]. In particular, the catalytic activity of mesoporous molecular sieves modified with Fe and its relationship with their magnetic properties have been reported [14,15] for the selective reduction of NO<sub>x</sub>.

In this work, mesoporous molecular sieves Si-MCM-41 have been synthesized and modified with Fe by the wet impregnation method. In addition, these materials were submitted to a high temperature reduction process to generate Fe-containing species in different oxidation states on the surface. These catalysts were evaluated in the cyclohexene oxidation with H<sub>2</sub>O<sub>2</sub>. Special attention was paid to the reaction product selectivity as a function of the treatment performed on the samples, and the catalytic behavior was related with the observed magnetic properties.

## 2. Experimental procedures

### 2.1. Synthesis

The pure siliceous mesoporous material (Si-MCM-41) was synthesized by using cetyltrimethylammonium bromide (CTAB) as template and tetraethoxysilane (TEOS) (Aldrich 98%) as silicon source. Sodium hydroxide (NaOH) aqueous solution 2 M was used for hydrolysis and pH adjustment. The catalyst was synthesized from gel of molar composition: NaOH/Si = 0.50, surfactant/Si = 0.12, water/Si = 132. In a typical synthesis, CTAB was dissolved in water–NaOH solution at 313 K; this new solution was then cooled to room temperature and TEOS was finally incorporated. The mixture was vigorously stirred for 4 h at room temperature and then for 3 h at 343 K in a closed flask. The final solid was filtered, washed and dried at 333 K overnight. To remove the template, the sample was heated (heating rate of 2 K/min) under N<sub>2</sub> flow up to 773 K and kept at this temperature for 6 h; it was then calcined under air flow for 6 h at 773 K.

The Si-MCM-41 host was then modified with Fe by the wet impregnation method. In order to obtain two different metallic loadings, an appropriate amount of none-hydrate iron (III) nitrate (Fe(NO<sub>3</sub>)<sub>3</sub>·9H<sub>2</sub>O) aqueous solution 2 or 5 M was added to the out gassed Si-MCM-41 (5 h in oven at 773 K). Then, water was slowly removed by rotary evaporation at 323 K for 30 min. The resulting powder was dried at 333 K and then calcined for 6 h at 773 K. Some of these samples were reduced in a H<sub>2</sub> flow of 50 mL/min. The samples were placed in a quartz reactor, heated at a rate of 10 K/min under H<sub>2</sub> flow up to 873 K and kept at this temperature for 6 h. The resulting materials were named: Fe/M(*x*) or Fe/M(*x*)R, where *x* is the initial concentration of the impregnating solution and R indicates that the sample was reduced.

### 2.2. Characterization

The X-ray diffraction (XRD) patterns were recorded in a Philips PW 3830 diffractometer with Cu K $\alpha$  radiation ( $\lambda = 1.5418 \text{ \AA}$ ) in the range of  $2\theta$  from 1.5 to 7° and from 10 to 70°. The interplanar distance ( $d_{(100)}$ ) was estimated using the position of the first X-ray diffraction line. The lattice parameter ( $a_0$ ) of the hexagonal

unit cell was calculated as  $a_0 = (2/\sqrt{3}) d_{(100)}$ . A profile fitting was made to each maximum in the high angle range, and the mean grain size [*D*] of the corresponding phase was estimated using the Scherrer formulae:  $[D] = 0.9\lambda/\beta \cos \theta$ , where  $\beta$  (in radians) is the peak intrinsic breadth after subtraction of the instrumental contribution,  $\lambda$  is the X-ray wavelength and  $\theta$  the diffraction (Bragg) angle.

UV–vis diffuse reflectance (DRUV–vis) spectra were recorded using an Optronic OL 750–427 spectrometer in the wavelength range 200–1000 nm. The original spectra obtained were fitted by three Gaussian bands using the conventional least squares method. Curve-fitting calculations were useful in determining each band location and relative area, with confidence levels given by  $\chi^2 \leq 0.0005$  and  $R^2 \geq 0.99$ . The Fe content was determined by atomic absorption spectroscopy (AA) using a Varian SpectrAA 220. Specific surface area, pore size distribution and total pore volume were determined from N<sub>2</sub> adsorption–desorption isotherms obtained at 77 K using a Quantachrome Autosorb Automated Gas Sorption System. The surface area was determined by the BET method in the pressure range of  $P/P_0$ : 0.01–0.25. The pore size distribution was calculated by the Barrett–Joyner–Halenda (BJH) method, based on the Kelvin equation [16]. Mössbauer spectra were recorded in transmission geometry using a constant acceleration spectrometer with a 50-mCi <sup>57</sup>CoRh source at room temperature.

The room temperature magnetization curves were measured in a vibrating sample magnetometer (VSM) LakeShore 7300, with static field up to  $\mu_0 H = 1.5 \text{ T}$ . Magnetization and hysteresis loops as functions of temperature were measured in a Quantum Design SQUID magnetometer up to 6 T. The hysteresis properties as coercivity and remanence were obtained directly from the magnetization curves; these hysteresis curves were well fitted by the sum of three contributions: a linear paramagnetic or diamagnetic contribution (LM), a ferromagnetic one (FM) [17], and a superparamagnetic-like one (SPM) [18], so that the total magnetization results:  $TM = LM + FM + SPM$ , with:

$$LM = \chi \mu_0 H_i \quad (1)$$

$$FM = \frac{2M_{sf}}{\pi} \left( \arctan \left( \frac{H_i + H_{ic}}{H_{ic}} \right) \tan \frac{\pi M_r}{M_{sf}} \right) \quad (2)$$

$$SPM = M_{ssp} \left\{ \coth h \frac{\mu(H_i + H_i^*)}{k_B T} - \frac{k_B T}{\mu(H_i + H_i^*)} \right\} \quad (3)$$

here  $M_{sf}$ ,  $\mu_0 H_{ic}$  and  $M_r$  are the effective ferromagnetic saturation magnetization, the coercive field and the remanent magnetization, associated to the ferromagnetic contribution, respectively.  $M_{ssp}$ ,  $\mu_i$  and  $H_i^*$  are the effective saturation magnetization, the mean magnetic moment of the activated clusters and a mean interaction field [18], introduced to account for the effect of eventual interactions between particles on the superparamagnetic-like component of the  $M(H)$  loops.

The temperature dependence of the magnetization was measured following the conventional zero field cooling (ZFC) and field cooling (FC) protocols, under a small applied field of 10 mT.

### 2.3. Catalytic experiments

The cyclohexene oxidation reactions with H<sub>2</sub>O<sub>2</sub> were carried out at 343 K, under vigorous stirring, in a batch reactor immersed in a thermostatic bath. Typically, the reacting mixture consisted of 9.00 mg of catalyst, 91.90 mg of cyclohexene (Baker 98%), 26.60 mg of oxidant (hydrogen peroxide 35% (w/w), Riedel-de Haen) and 678.30 mg of solvent (acetonitrile, Cicarelli). The substrate to oxidant molar ratio was 4:1 or 2:1. Samples were withdrawn at different times and analyzed by gas chromatography (Hewlett Packard 5890 Series II) using a capillary column (cross-linked

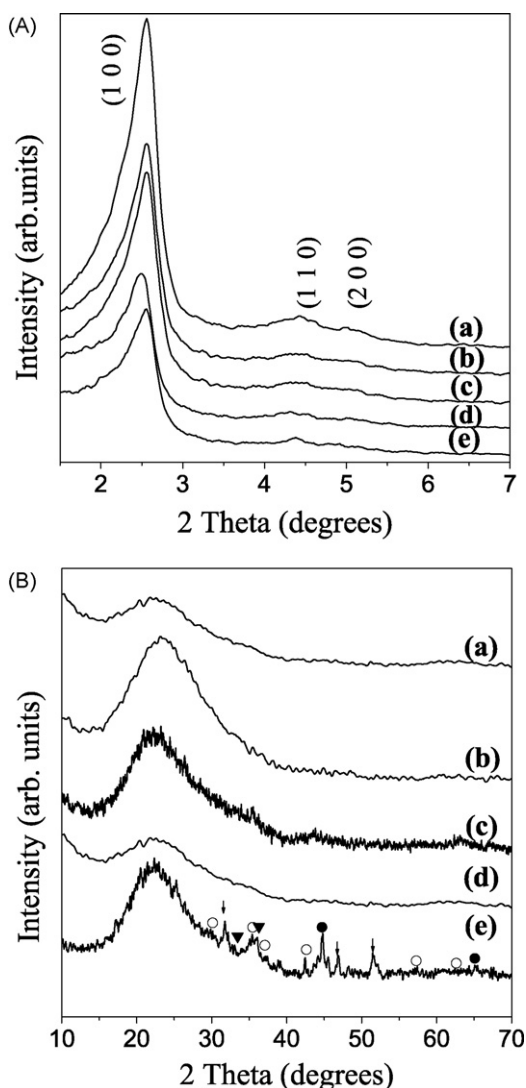


Fig. 1. XRD patterns of the samples: (a) Si-MCM-41, (b) Fe/M(2), (c) Fe/M(2)R, (d) Fe/M(5) and (e) Fe/M(5)R. (●) Fe, (○) Fe<sub>3</sub>O<sub>4</sub>, (▼) Fe<sub>2</sub>O<sub>3</sub> and (↓) unidentified specie.

methyl-silicone gum, 30 m long) and flame ionization detector. Additionally, the GC-MS (Shimadzu-QP 5050 A) analyzes were performed in order to identify the reaction products. The total conversion of H<sub>2</sub>O<sub>2</sub> was measured by iodometric titration. The cyclohexene conversion, named  $x_c$ , was defined as the ratio of the converted species to the initial cyclohexene concentration. Considering that the substrate to oxidant molar ratios were 4:1 and 2:1, it is important to state that the maximum possible cyclohexene conversion (maximum amount of the oxygenated products that could be obtained if all H<sub>2</sub>O<sub>2</sub> were consumed) is 25 and 50 mol%, respectively. The efficiency of H<sub>2</sub>O<sub>2</sub> was calculated as: moles of oxidized cyclohexene  $\times$  100%/moles of hydrogen peroxide converted.

Table 1

Structure properties and chemical composition of the mesoporous molecular sieves synthesized.

Sample	Fe content (wt.%)	Surface area (m <sup>2</sup> /g)	V <sub>p</sub> (cm <sup>3</sup> /g)	D <sub>p</sub> (nm)	a <sub>0</sub> (Å)	t (Å)
Si-MCM-41	–	1182	0.67	2.34	40.00	16.60
Fe/M(2)	3.78	911	0.51	2.17	40.96	19.26
Fe/M(2)R	3.65	553	0.32	2.10	39.69	18.69
Fe/M(5)	6.39	858	0.49	2.19	40.64	18.74
Fe/M(5)R	6.45	492	0.28	2.18	39.53	17.73

V<sub>p</sub>: pore volume; D<sub>p</sub>: pore diameter; t: wall thickness = (D<sub>p</sub> – a<sub>0</sub>).

The turnover number (TON) was defined as moles of cyclohexene converted/moles of Fe in the catalyst.

### 3. Results and discussion

#### 3.1. Structural and textural characterization

Fig. 1A shows the low angle XRD patterns for the Si-MCM-41 host and the impregnated samples before and after the reduction treatment. Three maxima are clearly observed for the Si-MCM-41 host, indexed as (100), (110) and (200) reflections, characteristic of a highly ordered mesoporous structure with hexagonal pore array. The low angle XRD patterns of all the iron loaded samples are similar to that of the Si-MCM-41 host, indicating that the MCM-41 structure was preserved after iron loading and the further reduction treatment. However, when the iron loading increases and mainly after the reduction treatment, the peaks broaden and their intensities decrease, indicating that some reduction in the long-range order of the structure takes place. The lattice parameter of the hexagonal unit cell (a<sub>0</sub>), together with other structural and chemical properties of the molecular sieves synthesized, is listed in Table 1. At large angles (Fig. 1B), no obvious diffraction peaks corresponding to crystalline iron oxides can be observed for the samples Fe/M suggesting that the iron oxide species, if any, are clusters or particles too small to be detected by XRD (crystallites smaller than about 5 nm). The XRD patterns corresponding to samples submitted to the reduction treatment indicate that Fe<sup>+3</sup> species (mainly Fe<sub>2</sub>O<sub>3</sub>) were partially reduced; the peaks corresponding to iron species with minor oxidation states insinuate in Fe/M(2)R and are clearly defined in the Fe/M(5)R sample. Larger particles are detected by XRD in the sample with the high iron content after the treatment under H<sub>2</sub> at high temperature; in fact, nano-crystals of metallic Fe<sup>0</sup> and Fe<sub>3</sub>O<sub>4</sub> (magnetite) could be identified besides the Fe<sub>3</sub>O<sub>2</sub> particles, with mean sizes between 13 ± 2 and 23 ± 5 nm. Meanwhile, in the less loaded and reduced sample (Fe/M(2)R) the mean size of hematite crystallites is below 10 nm. Therefore, it is likely that during the reduction process small Fe species migrate and coalesce forming larger particles on the external powder grain surfaces.

Fig. 2 shows in A the N<sub>2</sub> adsorption–desorption isotherms and in B the pore size distribution corresponding to the synthesized powders; the corresponding physical parameters are collected in Table 1. All the samples exhibit type IV isotherms typical of mesoporous structures, with a sharp inflection at relative pressure around 0.15–0.25, characteristic of capillary condensation inside the regular mesopores of the MCM-41 structure. Such inflection also provides clear evidence for a narrow pore size distribution in these materials, as it can be seen in Fig. 2B [6]. However, whereas this inflection is sharp for the Si-MCM-41 host, it becomes less pronounced when metal loading increases or the reduction treatment is applied, in agreement with the loose of structural order detected by XRD. In this sense, it is noteworthy that the sample Fe/M(5)R shows the largest hysteresis loop, which may be attributed to particle–particle porosity, to some large pores or to some mesopore disorder in shape [6].

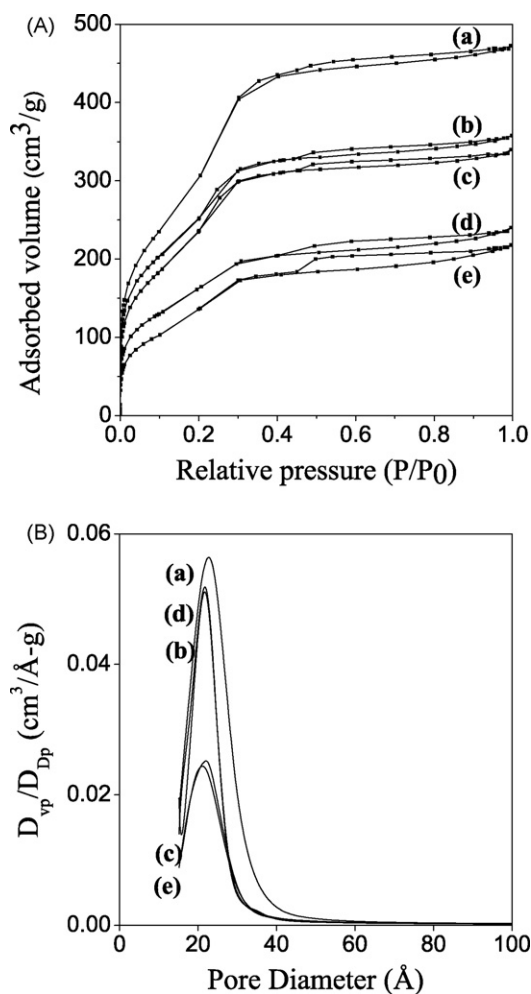


**Fig. 2.** (A) Nitrogen adsorption–desorption isotherms and (B) pore size distribution of samples: (a) Si-MCM-41, (b) Fe/M(2), (c) Fe/M(2)R, (d) Fe/M(5) and (e) Fe/M(5)R.

From the difference between pore diameter ( $D_p$ ) and the cell parameter  $a_0$  obtained by XRD, it is possible to estimate the wall thickness of the structure [6]. As shown in Table 1, the wall thickness for iron loaded samples is large, as compared to that of Si-MCM-41 host. This feature may be explained by the presence of clusters or very small particles of iron oxide (not detectable by XRD) finely dispersed inside the MCM-41 channels which would also be contributing to a decrease in the pore volume and surface area. However, even when the Fe loading reduces the pore volume and the surface area, in comparison with the Si-MCM-41 host, samples Fe/M(2) and Fe/M(5) exhibited areas and pore volumes typical of mesoporous materials, respectively. In reduced samples, a smaller wall thickness and a significant reduction in both the area and the pore volume are observed, as compared with the as calcined samples. These facts are consistent with the formation and further coarsening of nano-particles on the external surface during the high temperature reduction treatment. These large particles,

well detected by XRD, are likely to nucleate and grow at expenses of iron-oxygen nano-clusters and smaller nano-particles located on the pores internal surface [19]. Such large nano-particles, located on the external surface of the samples, would cause pore blocking, leading to the sharp drop in the pore volume, surface area and structure regularity.

### 3.2. Chemical characterization

DRUV-vis spectroscopy is a useful method to characterize the coordination environment of transition metals in zeolite type frameworks [20,21]. The DRUV-vis spectra of the investigated samples are shown in Fig. 3. The original spectra were fitted with three bands at about 220–250, 330–380 and 510–530 nm. The first maximum, associated with the  $d\pi-p\pi$  charge transfer between Fe and O [22,23] respectively, indicates that some iron atoms are able to link to O atoms, being incorporated into the host framework as isolated  $Fe^{+3}$  cations. The contributions detected at longer wavelengths evidence that iron is also present with octahedral coordination in extra-framework positions. Thus, the second maximum may be attributed to small oligonuclear  $(FeO)_n$  clusters [1,22–24], whereas the broad band at 510–530 nm may be assigned to larger iron oxide nano-particles [24,25]. It is known that the UV bands shift to higher wavelengths when the iron-oxygen nano-clusters or iron oxide nano-particles size increase, indicating a quantum size effect in these species. It is noticeable that the long wavelength absorption (between 300 and 700 nm) in the as calcined samples increases with Fe loading, accounting for the dominant presence of both iron-oxygen containing clusters and iron oxide nano-particles (sample Fe/M(5)). When sample Fe/M(2) is reduced the intensity of the first maximum slightly decreases and the absorption between 400 and 700 nm increases, for sample Fe/M(5)R, a clear decrease in the absorption between 200 and 300 nm is observed together with an increase in the peak areas. The shift of the last maximum towards higher wavelengths further confirms the mentioned quantum size effect and indicates that the reduction process favors the growth of larger nano-sized iron oxides. Therefore, we suggest that the iron species diffuse/migrate from the framework and/or from positions inside the channels toward the external surface to form larger iron oxides particles, being this process enhanced by the reduction conditions: a  $H_2$  flow and high temperature.

The room temperature Mössbauer spectra for the samples synthesized in this work are shown in Fig. 4 and the corresponding hyperfine parameters obtained by fitting the spectra are listed in Table 2. The as calcined samples present two doublets, with isomeric shifts ( $\delta$ ) and quadrupole splittings ( $\Delta Q$ ) characteristic of trivalent iron ions ( $Fe^{3+}$ ) in octahedral coordination ( $\delta$ : 0.316 and 0.306 mm/s;  $\Delta Q$ : 0.72 and 1.24/1.41 mm/s [26,27]). Considering these values, the contributions can be assigned to superparamagnetic nano-crystals of  $Fe_2O_3$  or/and small iron-oxygen clusters, also superparamagnetic, as well as to paramagnetic  $Fe^{+3}$  ions inserted in the mesostructure [28].

The spectra corresponding to the reduced samples show, besides the doublets already present in the as calcined samples, other doublets with  $\delta = 1.006$  and 0.886/1.116 mm/s and  $\Delta Q = 2.33$

**Table 2**  
Mössbauer parameters of the Fe-containing mesoporous molecular sieves.

Sample	$I_1 (Fe^{3+})$		$I_2 (Fe^{3+})$		$I_3 (Fe^{2+})$		$I_4 (Fe^{2+})$		$I_5$ (metallic Fe)		
	$\delta$ (mm/s)	$\Delta Q$ (mm/s)	$\delta$ (mm/s)	$\Delta Q$ (mm/s)	$B$ (mm/s)						
Fe/(2)M	0.316	0.72	0.306	1.24	–	–	–	–	–	–	–
Fe/(2)MR	0.346	0.96	–	–	1.006	2.33	–	–	–0.014	0.00	5.33
Fe/(5)M	0.316	0.72	0.306	1.41	–	–	–	–	–	–	–
Fe/(5)MR	0.366	0.95	–	–	0.886	2.32	1.116	2.81	–0.014	0.00	5.32

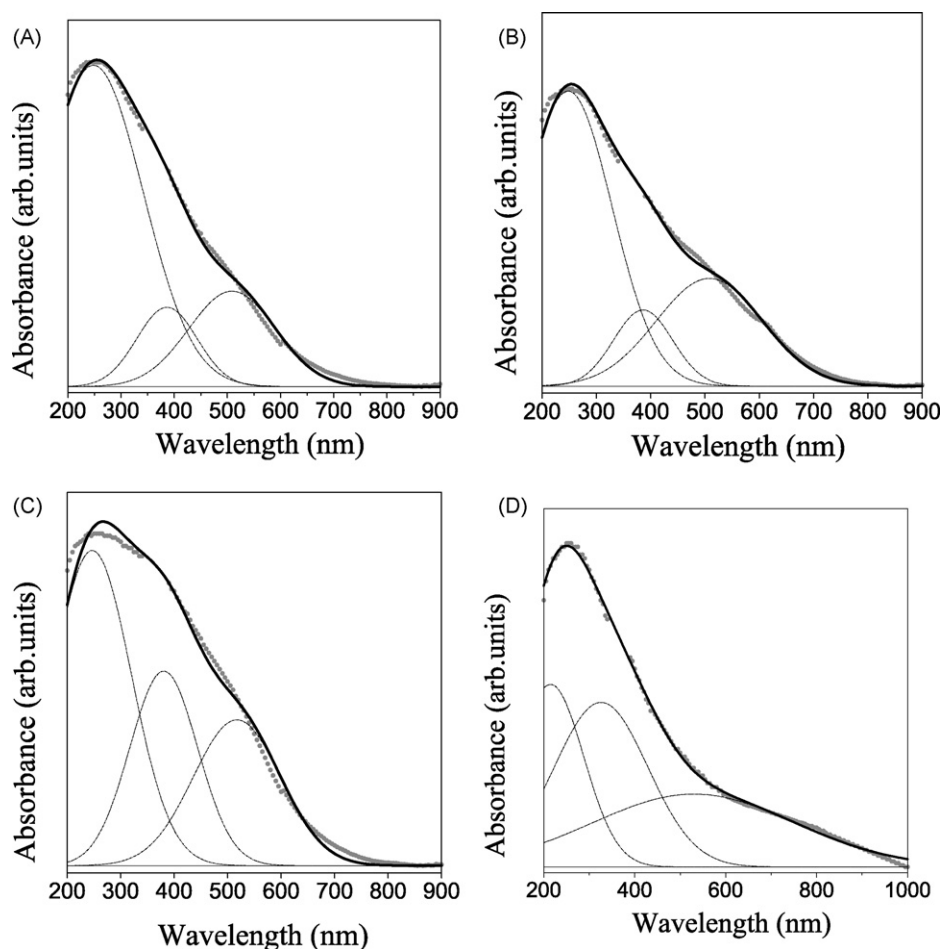


Fig. 3. DRUV-vis spectra of samples (A) Fe/M(2), (B) Fe/M(2)R, (C) Fe/M(5) and (D) Fe/M(5)R. Dotted: fitted curves; solid: experimental data.

and 2.32/2.81 mm/s for the samples Fe/M(2)R and Fe/M(5)R, respectively. These values are typical for Fe (II) ions in octahedral state and are considered as arising in superparamagnetic Fe<sub>3</sub>O<sub>4</sub> nano-particles [29]. It is worth to note that a good fitting could

be obtained for the sample by considering only one contribution (interaction), but two interactions were necessary to describe the spectrum of sample Fe/M(5)R. This is probably due to a minor iron content or smaller particle size in sample Fe/M(2)R.

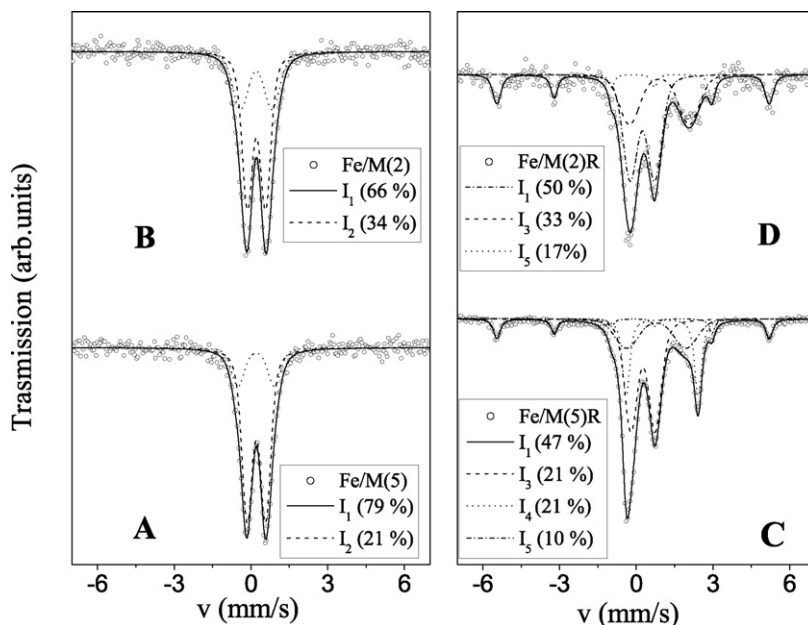
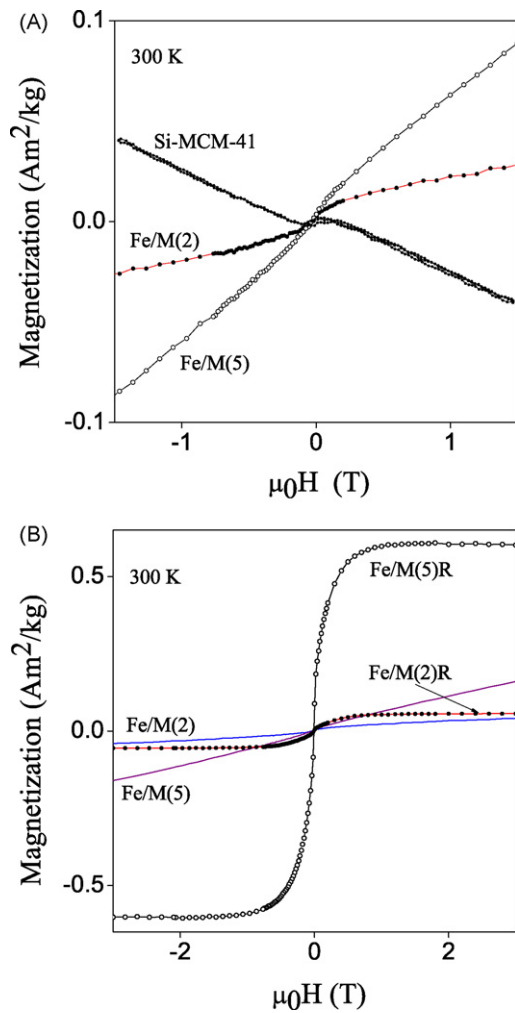


Fig. 4. Mössbauer spectra for samples (A) Fe/M(2), (B) Fe/M(2)R, (C) Fe/M(5) and (D) Fe/M(5)R. Lines correspond to the fitted curves.



**Fig. 5.** Room temperature hysteresis loops corresponding to samples: (A) Si-MCM-41, Fe/M(2) and Fe/M(5) and (B) Fe/M(2)R and Fe/M(5)R; the curves measured in the as calcined state are included for comparison.

In addition, reduced samples exhibit a sextet in the spectra, corresponding to an important fraction (10–17%) of metallic iron ( $\alpha$ Fe) with  $\delta$  and  $\Delta Q$  of  $-0.014$  and  $0$  mm/s. It should be noted that even when the  $\text{Fe}_3\text{O}_4$  and  $\text{Fe}^0$  species were identified by XRD in the sample Fe/M(5)R only, they are detected by Mössbauer spectroscopy in both reduced samples. This confirms that such species are also present in the sample Fe/M(2)R but with mean size smaller than 5 nm.

### 3.3. Magnetic properties

Fig. 5A shows the room temperature hysteresis loops corresponding to the Si-MCM-41 host and the as calcined Fe/M(2) and Fe/M(5) samples. For comparison, the room temperature loops corresponding to the reduced samples are showed in Fig. 5B. The magnetization curves recorded at different temperatures between 5 and 300 K, with applied fields up to 3 T, are depicted in Figs. 6 and 7. A first observation is that the iron modified materials are no longer diamagnetic, but show a mixed para-, superpara- and even ferromagnetic (Fe/M(5)R) character. The fact that no pure para- or superparamagnetic behavior is obtained becomes confirmed by the lack of curve collapse to a master curve when plotting the hysteresis loops measured at different temperatures, in reduced coordinates  $M/M_s$  and  $H/T$ , with  $M_s$  is the saturation magnetization,  $H$  is the applied field and  $T$  is the absolute temperature. In the

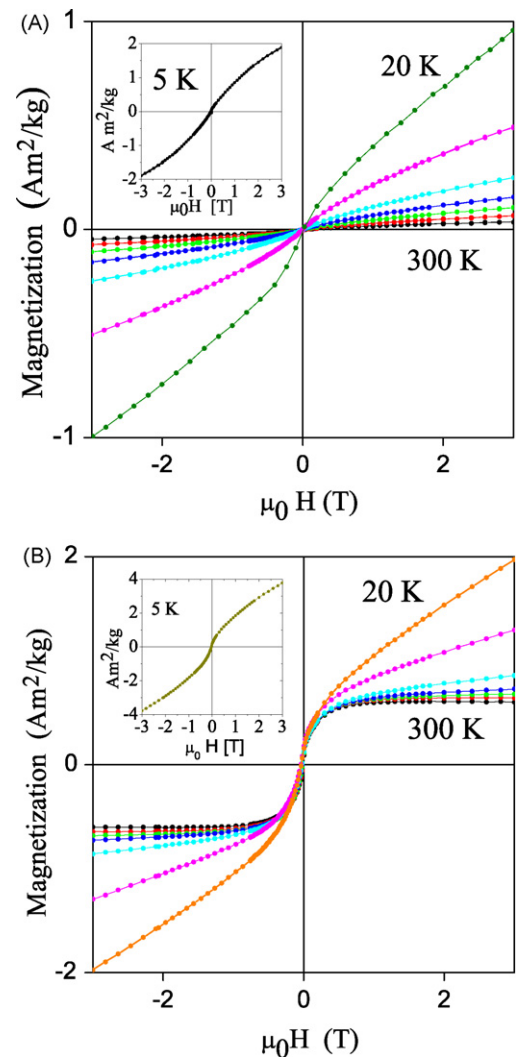


**Fig. 6.** Hysteresis loops measured at different temperatures for samples Fe/M(2) (A) and Fe/M(2)R (B). The maximum magnetization monotonously increases from 300 to 5 K. Intermediate temperatures are 250, 200, 150, 100, 50 and 20 K.

reduced samples the magnetization curves are described by the sum of two contributions: a ferromagnetic and a superparamagnetic one, following the Eqs. (2) and (3). In the case of the largest iron loading, the saturation magnetization largely increases after the reduction treatment at high temperature; this is mainly due to the apparition of  $\text{Fe}_3\text{O}_4$  and metallic Fe, as it is evidenced by Mössbauer spectroscopy and by the high angle XRD peaks observed in the Fe/M(5)R sample.

The temperature dependence of the magnetic parameters, obtained by fitting Eqs. (1)–(3) to the measured data, is summarized in Fig. 8A–D. The major contribution to the magnetization in the as calcined samples (Fe/M(2) and (Fe/M(5)) is paramagnetic, with a susceptibility largely increasing at low temperature (Fig. 8A). The second contribution is superparamagnetic, arising in small clusters with apparent mean magnetic moment about  $2000\mu_B$  in Fe/M(2) and  $20\mu_B$  in Fe/M(5). This apparent moment is found to decrease as temperature decreases, except in Fe/M(5), where it shows very low values in all the temperature range investigated (Fig. 8B). These differences may be attributed to clusters with different compositions as a result of the distinct iron loadings. The magnetization in the calcined and high temperature reduced samples (Fe/M(2)R and Fe/M(5)R) has two contributions, a paramagnetic and a ferromagnetic one. The apparent coercive field is found to increase as

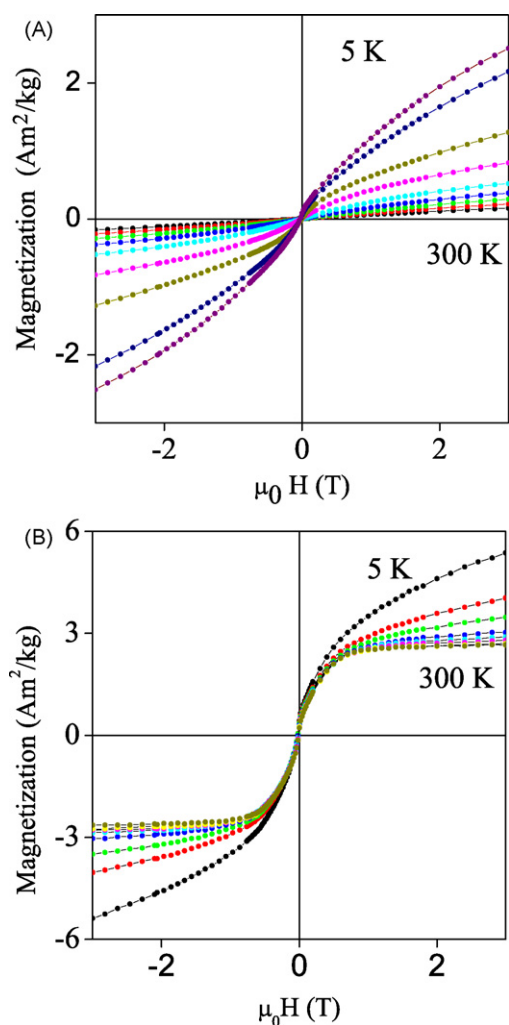


**Fig. 7.** Hysteresis loops measured at different temperatures for samples Fe/M(5) (A) and Fe/M(5)R (B). The maximum magnetization monotonously increases from 300 to 5 K. Intermediate temperatures are 250, 200, 150, 100, 50, 20, 14 and 7 K.

temperature decreases (Fig. 8C), reaching values of about 60 mT near 5 K.

Figs. 9 and 10 show the temperature dependence of the magnetization during ZFC and FC measurements, under an applied field of 10 mT. All the curves show a paramagnetic divergence as  $T \rightarrow 0$  indicating that in all the cases iron ions are inserted in the silica framework. The curves corresponding to sample Fe/M(2) show no heating-cooling hysteresis, as expected for paramagnetic or very small superparamagnetic units (clusters) with blocking temperature below 5 K. In the case of the higher iron loading (Fe/M(5)) a large superparamagnetic contribution is observed, with a mean blocking temperature close to 17 K. In samples reduced at high temperature, the magnetization also increases as  $T \rightarrow 0$  but now, new features are observed as a relatively large ZFC-FC hysteresis and a non-monotonic magnetization increase during cooling. In sample Fe/M(2)R, ZFC and FC magnetizations go both through a maximum near 200 K while in sample Fe/M(5)R the magnetization continuously increases during heating above 20 K up to room temperature as if the maximum were above 300 K. This behavior seems connected with large, ferromagnetic particles. The fact that both curves (ZFC and FC) go through a maximum has been attributed to a magnetic transformation or, in cases where no transformation is expected, to inter-particle interactions [30].

The results related to the catalytic activity of these iron modified molecular sieves are presented in Table 3. The actual Fe content,

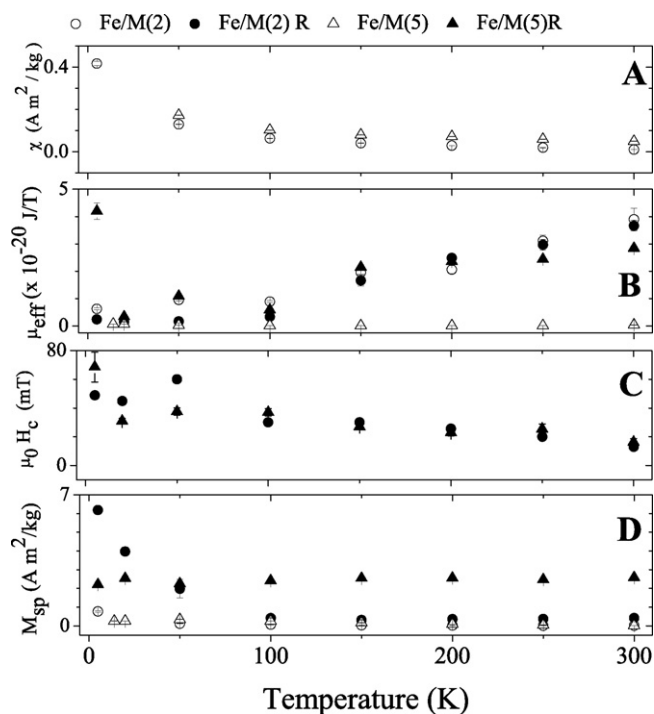
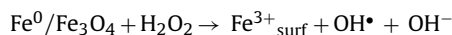


**Fig. 8.** Temperature dependence of (A) the paramagnetic susceptibility ( $\chi$ ), (B) the mean magnetic moment of superparamagnetic particles ( $\mu$ ), (C) the apparent coercive field ( $\mu_0 H_c$ ) and (D) the paramagnetic saturation magnetization  $M_{sp}$ , estimated by fitting Eqs. (1)–(3) to the data in Figs. 6 and 7.

determined by AA, is listed between parentheses. In all the cases an excess of substrate was employed to avoid the metal leaching. It is observed that in the case of as calcined samples and for both substrate oxidant ratios (4:1 and 2:1), the cyclohexene conversion ( $\chi_c$ ) is not modified by increasing Fe loads. Moreover, the catalyst with the higher Fe load (Fe/M(5)) shows smaller TON values, accounting for its lower effectiveness. Meanwhile, the peroxide conversion ( $\chi_{H_2O_2}$ ) increases with iron loading, but its efficiency decreases. These features may be attributed to the dominant presence, in sample Fe/M(5), of iron oxide clusters and/or nano-particles, both superparamagnetic, which could promote the  $H_2O_2$  decomposition. It is known that the presence of such extended M–O–M entities (M: transition metal) is primarily responsible for hydrogen peroxide decomposition [31].

When the catalysts are reduced, a slight increase in  $\chi_c$  besides an increase in  $\chi_{H_2O_2}$ , relative to the as calcined samples, was observed for both iron contents. Concerning the selectivity towards reaction products (Table 4), the reduced catalysts showed a quite different behavior with respect to as calcined samples. Thus, these reduced catalysts favor the formation of allylic oxidation products (III + IV) which reach selectivity values around 80%. It is known that these products arise from a radical path mechanism involving hydroxyl radicals. As it was evidenced by high angle XRD and Mössbauer spectroscopy, iron species with minor oxidation states such as  $Fe^0$  and  $Fe_3O_4$  appear when the as calcined samples are reduced. It has been reported that  $Fe^0/Fe_3O_4$  composites have a strong effect on the activity in the Fenton reaction, in which the generation of hydroxyl radicals is fundamental to reach the organic compound degradation [32]. The reaction mechanism has been discussed in terms of an easy electron transfer from  $Fe^0$  to the reaction medium via the  $Fe_3O_4$  to form  $HO^\bullet$  radicals by the Haber-Weiss reaction:



The high reactivity of  $Fe^0$  towards the  $H_2O_2$  decomposition found in these composites can be attributed to its special inter-

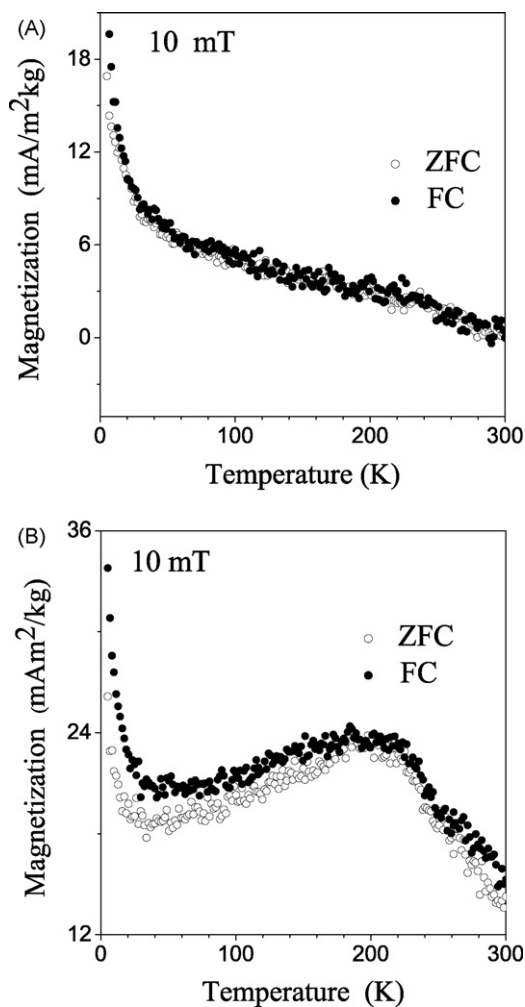


**Fig. 9.** Temperature dependence of the magnetization in the ZFC and FC states for an applied field of 10 mT in samples: (A) Fe/M(2) and (B) Fe/M(2)R.

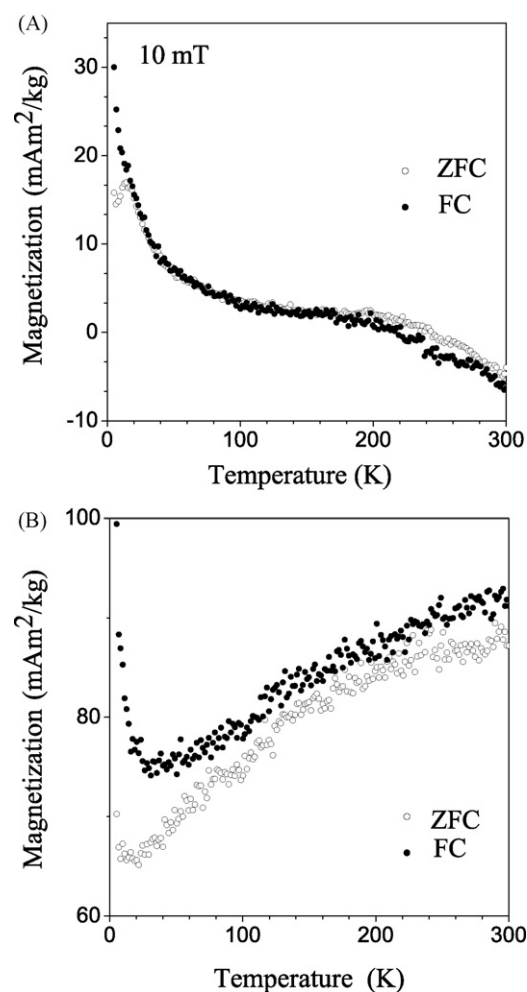


**Fig. 10.** Temperature dependence of the magnetization in the ZFC and FC states for an applied field of 10 mT in the samples (A) Fe/M(5) and (B) Fe/M5(R).

action with  $\text{Fe}_3\text{O}_4$ , which promote the electron transfer from  $\text{Fe}^0$  by acting as an intermediate/interface. In this mechanism the electron is initially transferred from  $\text{Fe}^0$  to  $\text{Fe}^{3+}_{\text{surf-magnetite}}$ , to produce/regenerate  $\text{Fe}^{2+}_{\text{surf-magnetite}}$  which would be the active sites for the reaction.

Therefore, the reaction of the species  $\text{Fe}^0/\text{Fe}_3\text{O}_4$ , with the peroxide in our reduced samples, would be accounting for the increase in the  $x_{\text{H}_2\text{O}_2}$ ; the generation of hydroxyl radicals would be responsible for the higher selectivity towards the allylic oxidation products.

Comparing the activity of the reduced samples as a function of iron loading, the fact that the  $x_c$  does not increase for sample Fe/M(5)R could be related to the formation of large ferromagnetic particles. It is well known that small metallic iron and magnetite

particles promote an increased reactivity towards electron transfer reactions [33]. Therefore the higher activity (higher TON value) observed in sample Fe/M(2)R should be related to the small size of  $\text{Fe}^0$  and  $\text{Fe}_3\text{O}_4$  particles (no detectable by XRD), with mainly superparamagnetic character, produced by reduction with  $\text{H}_2$ .

On the other hand, although the experiments carried out using a substrate to oxidant molar ratio of 2:1 allowed reaching a higher alkene conversion, the  $\text{H}_2\text{O}_2$  efficiency decreased as a consequence of its higher decomposition. Moreover, an increase in the 1,2-cyclohexanediol (**II**) selectivity was observed. This product arises from epoxide ring opening reactions which would be favored by the higher peroxide concentration.

**Table 3**

Catalytic activity of the Fe-containing mesoporous molecular sieves in the cyclohexene oxidation reaction.

Sample	$\text{C}_6\text{H}_{10}/\text{H}_2\text{O}_2$ (mol/mol)	$x_c$ (mol %)	$x_{\text{H}_2\text{O}_2}$ (mol %)	$\text{H}_2\text{O}_2$ efficiency (%)	TON
Fe/M(2) (3.78)	4:1	10.62	56.86	74.53	18.02
Fe/M(2) (3.78)	2:1	17.99	61.39	56.22	29.26
Fe/M(2)R (3.65)	4:1	11.72	67.68	69.29	19.91
Fe/M(5) (6.39)	4:1	10.43	62.48	67.6	10.11
Fe/M(5) (6.39)	2:1	16.83	63.14	47.06	15.64
Fe/M(5)R (6.45)	4:1	11.67	64.18	71.91	11.30

Reaction conditions: temperature: 343 K; reaction time: 5 h; catalyst = 9.79 wt.% of the substrate. The Fe content determined by AA is indicated between parentheses.

**Table 4**

Product selectivity for the cyclohexene oxidation by H<sub>2</sub>O<sub>2</sub> over the Fe-containing mesoporous molecular sieves.

Sample	C <sub>6</sub> H <sub>10</sub> /H <sub>2</sub> O <sub>2</sub> (mol/mol)	Products selectivity (mol%)			
		I	II	III	IV
Fe/M(2) (3.78)	4:1	6.35	39.49	39.13	13.53
Fe/M(2) (3.78)	2:1	6.10	51.51	30.35	9.98
Fe/M(2)R (3.65)	4:1	10.87	5.22	56.88	24.67
Fe/M(5) (6.39)	4:1	5.64	43.79	37.74	11.73
Fe/M(5) (6.39)	2:1	5.77	48.44	33.69	9.93
Fe/M(5)R (6.45)	4:1	10.07	10.63	58.93	18.42

Reaction conditions: temperature: 343 K; reaction time: 5 h; catalyst = 9.79 wt.% of the substrate. The Fe content determined by AA is indicated between parentheses.

#### 4. Conclusions

Iron-containing mesoporous molecular sieves have been successfully prepared by a wet impregnation procedure with Fe(NO<sub>3</sub>)<sub>3</sub> as precursor. It was found that the iron content and the reduction treatment carried out under H<sub>2</sub> flow strongly affect the structural properties and the nature of the Fe-containing species obtained, leading to samples with different magnetic behavior and catalytic activity. Although a lower degree of structural order was observed in samples with the high iron load (~6.5 wt.%), a good structure quality was obtained in all the cases. Iron deposited on these mesoporous silica templates was detected in the form of isolated Fe<sup>3+</sup> cations, oligonuclear (FeO)<sub>n</sub> clusters and bulky iron oxide nanoparticles. The presence of clusters or very small superparamagnetic iron oxide particles, finely dispersed inside the MCM-41 channels, would be responsible for the thicker walls as well as for the lower pore volume and surface area in iron loaded samples with respect to the Si-MCM-41 host. A further reduction process carried out under H<sub>2</sub> flow resulted in the formation of larger particles of different iron species with minor oxidation states (mainly Fe<sub>3</sub>O<sub>4</sub> and metallic iron) as it is evidenced by XRD, DRUV-vis and Mössbauer spectroscopy. Such partially reduced nano-particles, with superparamagnetic and ferromagnetic character, grow on the external surface of the material at expenses of nano-clusters and smaller nano-particles, located inside the pores, through a diffusion process. This migration and subsequent coarsening leads to a pronounced decrease in the surface area and pore volume, as observed after reduction. The materials synthesized showed good activity for the epoxidation of cyclohexene using H<sub>2</sub>O<sub>2</sub> as oxidant. For all the samples, an increase in the iron loading led to a decrease in the catalyst effectiveness. In the case of the calcined sample with higher iron content, nano-clusters and/or nano-particles of superparamagnetic hematite are likely to favor the H<sub>2</sub>O<sub>2</sub> decomposition, consequently decreasing its efficiency. On the other hand, the partially reduced species forming during the treatment under H<sub>2</sub> flow (mainly Fe<sup>0</sup> and Fe<sub>3</sub>O<sub>4</sub>) would be responsible for the generation of hydroxyl radicals, which largely increase the selectivity towards allylic oxidation products. However, the presence of large ferromagnetic particles in samples with high iron content may account for its lower catalytic activity. Finally, while an increase in the oxidant concentration allowed  $\alpha_c$  to increase, the H<sub>2</sub>O<sub>2</sub> efficiency

decreased due to its higher decomposition. Under these conditions the selectivity to 1,2-cyclohexanediol (II) is increased as a result of epoxide ring opening.

#### Acknowledgements

G.A.E., S.G.C., K.S. and M.I.O. CONICET Researchers; V.R.E. and A.M.N. CONICET Doctoral Fellowships. This work was supported by the CONICET, UTN-FRC and Secyt-UNC of Argentina. The authors are grateful to Dra. Claudia Rodriguez Torres (UNLP-La Plata, Argentina) for Mössbauer Effect Spectroscopy results.

#### References

- [1] Y. Wang, Q. Zhang, T. Shishido, K. Takehira, J. Catal. 209 (2002) 186–196.
- [2] W. Carvalho, M. Wallau, U. Schuchardt, J. Mol. Catal. 144 (1999) 91–99.
- [3] A. Costa, G. Ghesti, J. Macedoa, V. Braga, M. Santos, J. Dias, S. Dias, J. Mol. Catal. 282 (2008) 149–157.
- [4] E. Serwicka, J. Poltowicz, K. Bahranowski, Z. Olejniczak, W. Jones, Appl. Catal. A: Gen. 275 (2004) 9–14.
- [5] W. Sanderson, Pure Appl. Chem. 72 (2000) 1289–1304.
- [6] G. Eimer, S. Casuscelli, G. Ghione, M. Crivello, E. Herrero, Appl. Catal. A: Gen. 298 (2006) 232–242.
- [7] K. Balkus Jr., A. Khanmamedova, J. Shi, Stud. Surf. Sci. Catal. 110 (1997) 999–1006.
- [8] R. Sever, R. Alcalá, J. Dumesic, T. Root, Micropor. Mesopor. Mater. 66 (2003) 53–67.
- [9] Y. Du, S. Liu, Y. Ji, Y. Zhang, F. Liu, Q. Gao, F. Xiao, Catal. Today 131 (2008) 70–75.
- [10] R. Hirsh, E. Katz, I. Willner, J. Am. Chem. Soc. 122 (2000) 12053–12054.
- [11] E. Katz, L. Ichia, I. Willner, Chem. Eur. J. 8 (2002) 4138–4148.
- [12] L. Ihia, E. Katz, J. Wasserman, I. Willner, Chem. Commun. (2002) 158–159.
- [13] Q. Pankhurst, R. Pollard, J. Phys.: Condens. Mater. 5 (1993) 8487–8508.
- [14] O. Anunziata, M. Gomez Costa, A. Beltramone, Appl. Catal. A 307 (2006) 263–269.
- [15] G. Fierro, M. Lo Jaconob, R. Dragonea, G. Ferrarisa, G. Andreozzi, G. Grazianic, Appl. Catal. B 57 (2005) 153–165.
- [16] E. Barrett, L. Joyner, P. Halenda, J. Am. Chem. Soc. 73 (1951) 373–380.
- [17] M. Stearns, Y. Cheng, J. Appl. Phys. 75 (1994) 6894–6898.
- [18] P. Allia, M. Coisson, M. Knobel, P. Tiberto, F. Vinai, Phys. Rev. B 60 (1999) 12207–12218.
- [19] O. Lebedeva, W. Sachtler, J. Catal. 191 (2000) 364–372.
- [20] S. Bordiga, S. Coluccia, C. Lamberti, L. Marchese, A. Zecchina, F. Boscherini, F. Bufo, F. Genoni, G. Leofanti, G. Petrini, G. Vlaic, J. Phys. Chem. 98 (1994) 4125–4132.
- [21] G. Ricchiardi, A. Damin, S. Bordiga, C. Lamberti, G. Spano, F. Rivetti, A. Zecchina, J. Am. Chem. Soc. 121 (2001) 11409–11419.
- [22] A. De Stefanis, S. Kaciulis, L. Pandolfi, Micropor. Mesopor. Mater. 99 (2007) 140–148.
- [23] Y. Lu, J. Zheng, J. Liu, J. Mu, Micropor. Mesopor. Mater. 106 (2007) 28–34.
- [24] S. Liu, Q. Wang, P. Van Der Voort, P. Cool, E. Vansant, M. Jiang, J. Magn. Mater. 280 (2004) 31–36.
- [25] L. Chmielarz, P. Kustrowski, R. Dziembaj, P. Cool, E. Vansant, Appl. Catal. 62 (2006) 369–380.
- [26] H. Pardoe, W. Chua-anusorn, T.G. St. Pierre, J. Dobson, J. Magn. Mater. 225 (2001) 41–46.
- [27] Y. Kuang, N. He, J. Wang, P. Xiao, C. Yuan, Z. Lu, Colloid Surf. A: Phys. Eng. Aspects 179 (2001) 177–184.
- [28] F. Bengoa, M. Cagnoli, N. Gallegos, A. Alvarez, L. Moggi, M. Moreno, S. Marchetti, Micropor. Mesopor. Mater. 84 (2005) 153–160.
- [29] L. Shiquan, Q. Wang, P. Van Der Voort, P. Cool, J. Magn. Mater. 280 (2004) 31–36.
- [30] R.D. Zysler, D. Fiorani, A.M. Testa, J. Magn. Mater. 224 (2001) 5–11.
- [31] C. Palazzi, L. Oliva, M. Signoreto, G. Strukul, J. Catal. 194 (2000) 286–293.
- [32] R. Costa, F. Moura, J. Ardisson, J. Fabris, R. Lago, Appl. Catal. B: Environ. 83 (2008) 131–139.
- [33] F. Moura, M. Araujo, J. Ardisson, W. Macedo, A. Albuquerque, R. Lago, J. Braz. Chem. Soc. 18 (2007) 322–329.